

Artificial Evolution Strategy for PET Reconstruction

Franck P. Vidal, Yoann L. Pavia, Jean-Marie Rocchisani, Jean Louchet, and Évelyne Lutton

Abstract—This paper shows new results of our artificial evolution algorithm for positron emission tomography (PET) reconstruction. This imaging technique produces datasets corresponding to the concentration of positron emitters within the patient. Fully three-dimensional (3D) tomographic reconstruction requires high computing power and leads to many challenges. Our aim is to produce high quality datasets in a time that is clinically acceptable. Our method is based on a co-evolution strategy called the “Fly algorithm”. Each fly represents a point in space and mimics a positron emitter. Each fly position is progressively optimised using evolutionary computing to closely match the data measured by the imaging system. The performance of each fly is assessed based on its positive or negative contribution to the performance of the whole population. The final population of flies approximates the radioactivity concentration. This approach has shown promising results on numerical phantom models. The size of objects and their relative concentrations can be calculated in two-dimensional (2D) space. In 3D, complex shapes can be reconstructed. In this paper, we demonstrate the ability of the algorithm to fidely reconstruct more anatomically realistic volumes.

Index Terms—Evolutionary computation, inverse problems, adaptive algorithm, Nuclear medicine, Positron emission tomography, Reconstruction algorithms.

I. INTRODUCTION

The core principle in nuclear medicine is to administer a radioactive substance called tracer to patients. It is absorbed by tissue in proportion to a physiological process. In oncology, it is the growth of tumour cells. The reconstruction allows the recovery of the 3D distribution of the tracer through the body (see Fig. 1(a)). There are two kinds of tomographic modality in nuclear medicine:

- Single-photon emission computed tomography (SPECT) makes use of gamma emitters, i.e. photons, as a radio-tracer.
- PET makes use of positron emitters. This is the modality that we will consider in this article.

Fig. 1(b) illustrate the PET acquisition process. After interactions, a positron combines with an electron. It generally produces two photons of 511 kiloelectron volt (keV) emitted in opposite directions. They are detected in ‘coincidence’ (i.e. almost at the same time). The line between the detectors that have been activated for a given pair of photons is called line of response (LOR).

F. Vidal and Y. Pavia are with the School of Computer Science, Bangor University, Dean Street, Bangor LL57 1UT, UK (e-mail: f.vidal@bangor.ac.uk).

J.-M. Rocchisani is with Université Paris 13 & Avicenne Hospital, Bobigny, France (e-mail: jeanmarie.rocchisani@avc.aphp.fr).

J. Louchet is with Ghent University (e-mail: jean.louchet@gmail.com).

É. Lutton was with AVIZ, INRIA Saclay-Île-de-France, France. She is now with MALICES, INRA-AgroParisTech, Thiverval-Grignon, France (e-mail: evelyne.lutton@grignon.inra.fr).

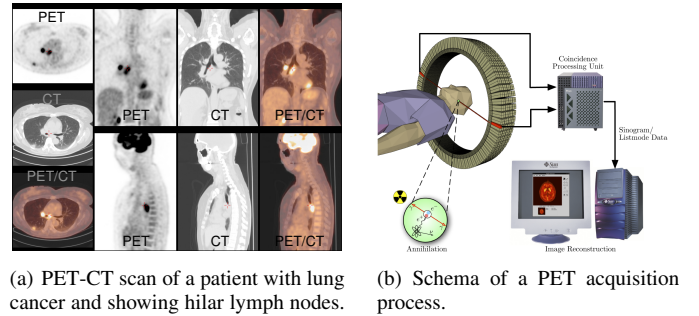


Fig. 1. PET imaging.

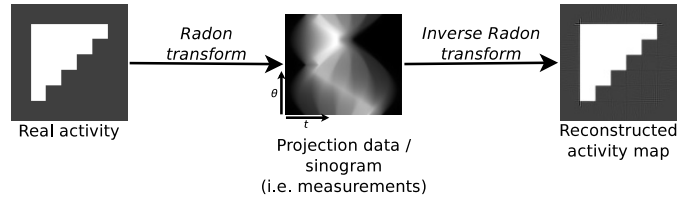


Fig. 2. Analytic reconstruction.

Section II presents background materials about tomography reconstruction using standard methods and preliminary results obtained using our cooperative coevolution strategy. Section III details the evolutionary algorithm that we developed for positron emission tomography reconstruction. New results and conclusions are presented in Section IV and V respectively.

II. BACKGROUND

A. Tomography Reconstruction

An overview of reconstruction methods in nuclear medicine can be found in [1]. They are often divided in two classes.

1) *Analytical methods*: They are based on a continuous modelling and the reconstruction process consists of the inversion of measurement equations (see Fig. 2). The most frequently used is the filtered back-projection (FBP) algorithm [2].

These reconstruction methods inverse the Radon transform. The projection data consists of the observed data. It is what is known and it corresponds to the Radon transform (or forward-projection) of the real activity. The real activity is unknown and the tomography reconstruction aims at recovering the activity. It is performed by using the Inverse Radon transform (or back-projection) to create an estimated activity map from the projections.

2) *Iterative statistical methods*: They are based on iterative correction algorithms (see Fig. 3) [3].

Iterative methods are relatively easy to model:

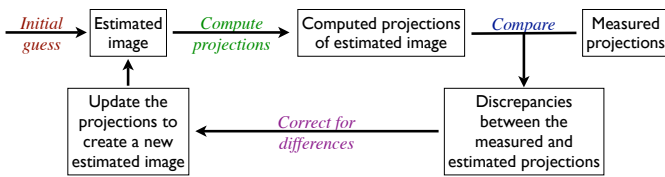


Fig. 3. Iterative method model.

- the reconstruction starts using an initial estimate of the image (generally a constant image),
- projection data is computed from this image,
- the estimated projections are compared with the measured projections,
- corrections are made to update the estimated image, and
- the algorithm iterates until a convergence threshold – between the estimated and measured projection sets – has been reached.

There are different ways to implement these iterative methods. The main differences are about the computation of the projections, how the physics corrections (scattering, random, attenuation, etc.) are applied, and how the error corrections are applied in the estimated projections.

The maximum-likelihood expectation-maximisation (ML-EM) [4] and ordered subset expectation-maximisation (OS-EM) [5] are the most widely used techniques PET. They are iterative methods. ML-EM assumes Poisson noise is present in the measured data. It does not produce the artefacts seen in classic FBP reconstructions, and it has a better signal-to-noise ratio in region of low concentration. However, the algorithm is known to converge rather slowly. OS-EM has been proposed to speed-up convergence of the expectation-maximisation (EM) algorithm and it has become the reference reconstruction method. Its principle is to reduce the amount of projections used at each iteration of the EM algorithm by subdividing the projections in K sub-groups. The projections of a sub-group are uniformly distributed around the volume to reconstruct.

ML-EM and its derivative, OS-EM are gold standard reconstruction techniques in nuclear medicine. These reference reconstruction methods, however, suffer from factors that limit the quantitative analysis of their results, hence limit their exploitation during the treatment planning process and during treatment monitoring.

Prior to the reconstruction, the LOR data is often rebinned into a sinogram [6], [7]. This intermediate data representation corresponds to projection data that can be used by conventional tomographic reconstruction codes. A broad overview of reconstruction methods using projection data in nuclear medicine can be found in [7], [8]. Using sinograms in PET introduces drawbacks (such as sampling, difficulties to take advantages of physics and geometrical properties of the imaging system, etc.) and, therefore, a new approach dedicated to PET is required to directly use the list-mode data. Other limiting factors include the use of noisy, large and complex datasets, complex physical phenomena (such as Compton scattering and gamma attenuation for example), and the movement of patients (including the motion of internal structures due to respiration).

It is possible to take them into account to attenuate the artefacts that they generate in reconstructed images, e.g. by ‘cleaning’ sinograms or writing dedicated correction algorithms for list-mode data, and this has been an active field of research for quite some time. However, these technologies are not readily available in the clinic, mainly because of the heavy computational power that they require and/or the difficulty of modelling all these corrections in standard algorithms.

B. Evolutionary reconstruction

The algorithm that we present here follows the iterative algorithm paradigm. Image reconstruction in tomography is an inverse problem that is ill-posed: a solution does not necessarily exist (e.g. in extreme cases of excessive noise), and the solution may not be unique. This problem can be solved as an optimisation problem, and on such cases, evolutionary algorithms (EAs) have been proven efficient in general, and in particular in medical imaging [9], [10], [11]. An EA is a stochastic optimisation tool that relies on Darwin’s principles to mimic complex natural behaviours [12]. In particular, it makes use of ‘genetic operators’ based on the biological mechanisms of natural evolution (e.g. reproduction, mutation, recombination, and selection). The candidate solutions to the problem to be solved by optimisation are called ‘individuals’. Individuals are grouped into a population. The population evolves using the repeated application of the genetic operators. The adequacy of an individual ‘to live’ in its environment is measured using a ‘fitness function’ (also called ‘cost function’). After convergence, the ‘best’ individual is extracted. It corresponds to the solution of the optimisation problem.

In preliminary studies, we introduced a cooperative co-evolution strategy (or “Parisian evolution”) called “fly algorithm” [13]. Cooperative-coevolution approaches rely on a formulation of the optimisation problem as a collection of interdependent subproblems. The population is thus made of simpler items, parts of a full solution, that “cooperate” to build the searched optimum. A Parisian EA (see Fig. 4) generally contains all the usual components of an EA, plus 2 levels of fitness:

- *Global fitness* computed on the whole population. It may be the sum (or a complex combination) of local fitnesses.
- *Local fitness* computed on each individual to assess their own contribution to the global solution. The local fitness of an individual may be defined as its marginal contribution to the global fitness.

Contrary to traditional EAs, the Fly algorithm embeds the searched solution within the whole population, letting each individual be only a part of the solution. The validity of this approach has been first demonstrated for SPECT reconstruction [14]. The searched distribution of radionuclides is modelled as a sample set of 3D points, the population of “flies”. For SPECT, each fly emits γ -photons. Using a cooperative co-evolution scheme to optimise the position of radionuclides, the population of flies evolves so that the data estimated from flies matches measured data. The final population approximates the radioactivity concentration (see Fig. 5 for an example in SPECT).

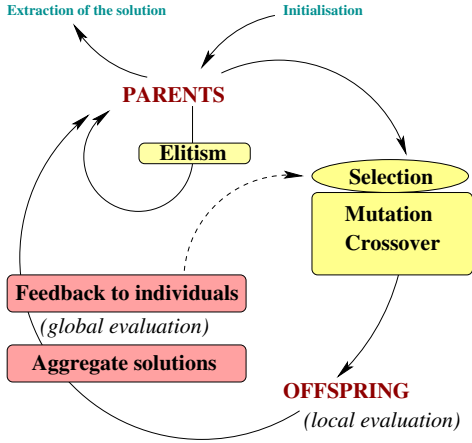


Fig. 4. Parisian approach principles.

TABLE I
FWHM IN MM ESTIMATED FROM FIG. 6.

	FWHM in Fig. 6(a) (reference)	FWHM in Fig. 6(b) (fly reconstruction)	Absolute difference
1	19	18	1
2	49	48	1
3	19	18	1
4	49	47	2
5	19	17	2

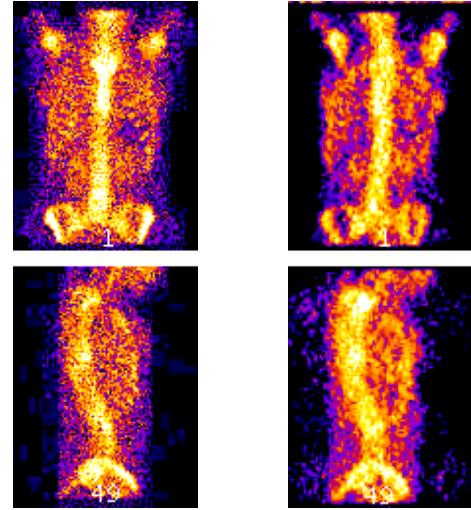
The approach has been extended to the more complicated case of PET reconstruction [15]. It showed promising results in relatively simple test cases in fully-3D LOR space [16], [17], [18], [19]. The size and relative concentration of objects can be retrieved (see Fig. 6 for an example in PET). Full width at half maximum (FWHM) is measured to quantify errors in Fig. 6 (see Table I). The error is smaller than the size of crystals, which is 4.5 mm (see Section IV for details about the simulated system geometry). Fig. 7 shows that complex shapes can also be reconstructed in fully-3D.

III. MATERIAL AND METHODS

As illustrated by the flow chart of our Fly algorithm for PET (see Fig. 8), the evolutionary scheme for tomography reconstruction follows the iterative paradigm (see Fig. 3). The steps of the iterative method, as of Fig. 3, can be described as follows:

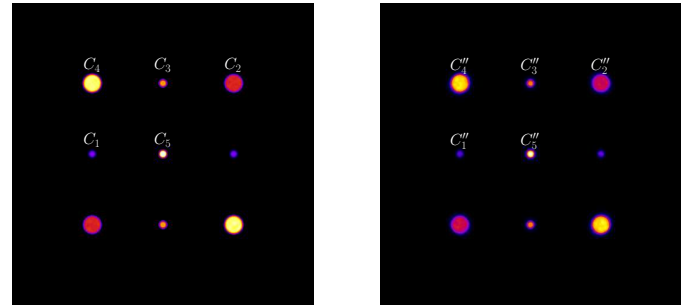
A. Initial guess

Each individual, or fly, corresponds to a 3D point. Initially, the flies' position is randomly generated in the volume within the scanner. Iterative reconstruction methods generally make use of a constant volume as an initial estimate of the volume (see Fig. 9(a)). However, to speed-up the reconstruction process, a volume is first reconstructed using a fast analytical algorithm, the simple back-projection, that we implemented on the graphics card using OpenGL. The algorithm consists in back-projecting each LOR into the volume space. Pixels along the path of a LOR are updated uniformly, i.e. without taking into account photon attenuation. This operation is fast and



(a) Reference image: acquired SPECT projections of a bone scan.
(b) Reconstructed data: projections of the reconstructed slices.

Fig. 5. Fly reconstruction in SPECT [14].



(a) Reference image.

(b) Reconstructed data.

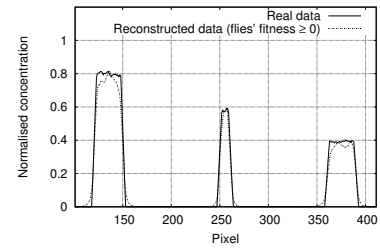
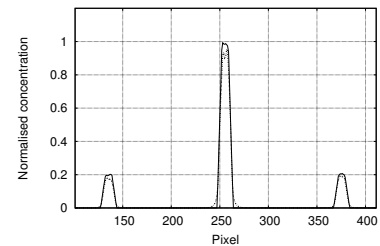
(c) profile: through the 1st line of cylinders.(d) profile: through the 2nd line of cylinders.

Fig. 6. PET reconstruction using the Fly algorithm: 9 cylinders having 2 different radii (1 cm and 2.5 cm) and 5 different radioactivity concentrations ($C_1 = 114,590$ count/ml, $C_2 = 2C_1$, $C_3 = 3C_1$, etc.) [17], [19].

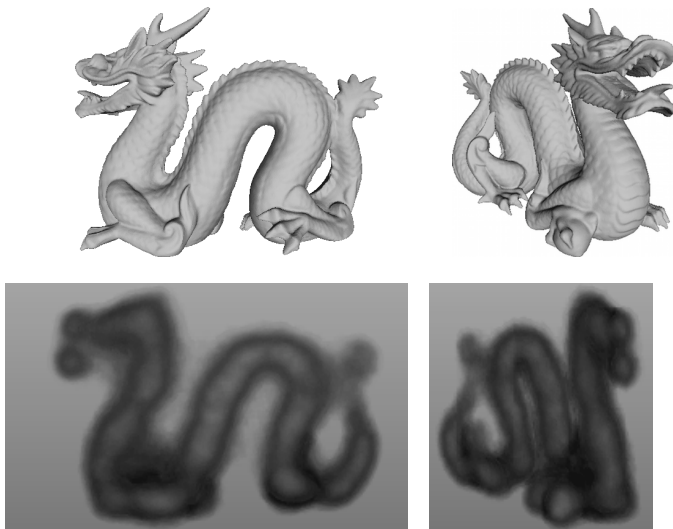


Fig. 7. Simulation performed using the dragon model from *The Stanford 3D Scanning Repository*, <http://graphics.stanford.edu/data/3Dscanrep/>. The object is uniformly filled with radiotracers (top row). The reconstructed radiotracer distribution is displayed using volume rendering (bottom row).

provides the evolutionary algorithm with an initial guess of the volume (see Fig. 9(c)). For each voxel of the initial estimate, a given number of flies is uniformly distributed depending on the voxel intensity (see Fig. 9(b)).

B. Compute projections

Each fly mimics a radioactive emitter, i.e. n stochastic simulations of annihilation events are performed to compute the fly's illumination pattern. For each annihilation event, a photon is emitted in a random direction. A second photon is then emitted in the opposite direction. If both photons are almost simultaneously detected by the scanner according to a coincidence time window, the corresponding LOR is recorded. The scanner properties (e.g. detector blocks and crystals positions) are modelled, and each fly is producing an adjustable number of annihilation events (see Fig. 10). Each fly keeps a record of its simulated LORs. Therefore the result of these simulations consists of a list, per fly, of pairs of detector identification numbers that correspond to LORs. These lists are aggregated to form the population total illumination pattern, which should closely match the data recorded by the PET scanner. They correspond to sparse matrices containing coincidence data.

C. Compare

The global fitness function used during the selection operation measures the discrepancies between the simulated projections and the real projections (see [19] for details about our specific genetic operators and the fitness metric). The City block distance between the two sparse matrices has been chosen as it provides a good compromise between accuracy and speed. The aims of the evolutionary algorithm is to minimise the global fitness function, i.e. the distance between these two sets of data. The smaller the distance is, the closer the reconstructed data will be to the real radioactive activity.

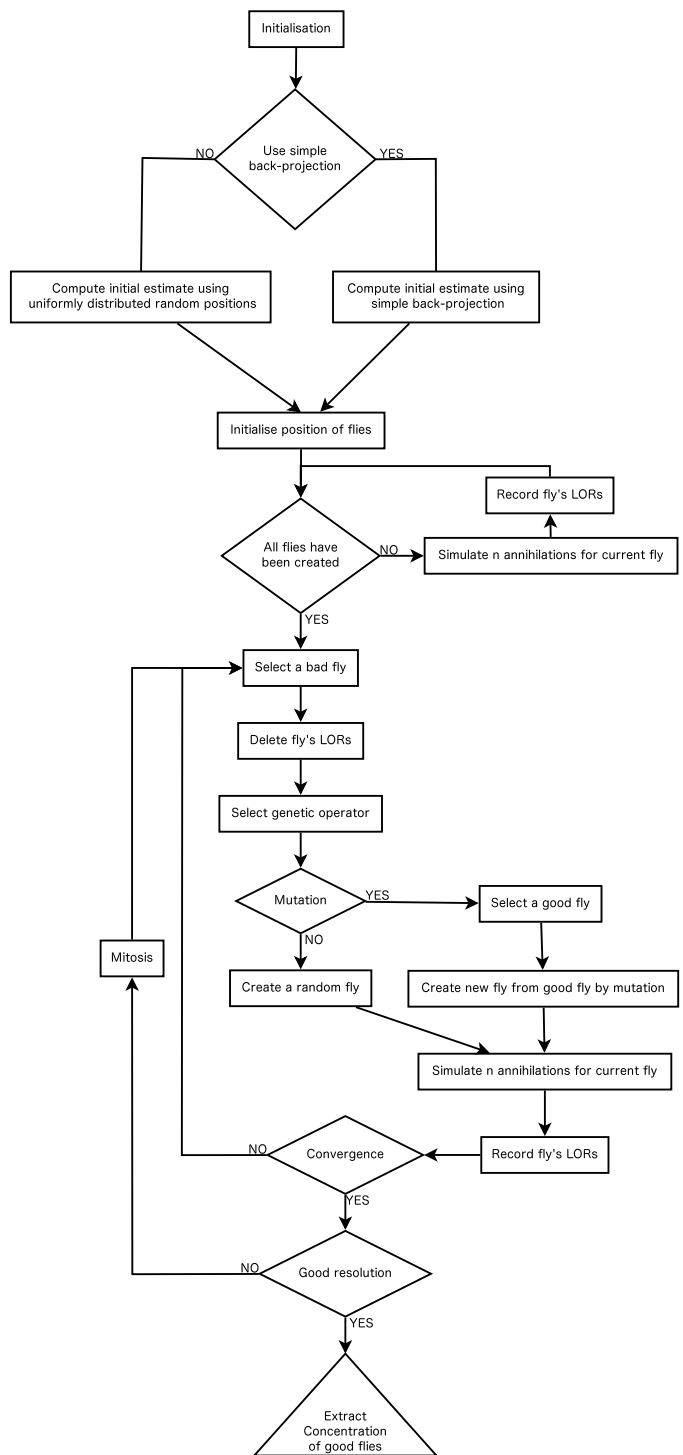


Fig. 8. Flow chart of the PET reconstruction using the Fly algorithm.

D. Correct for differences

The optimisation of the radioactive emitter positions is performed using genetic operations instead of the EM method. The population of flies evolves so that the population total pattern matches measured data. We chose to implement a “steady state” evolutionary strategy, in which at each loop one individual (fly) has to be eliminated and replaced with a new fly. The fly to be killed is randomly chosen by the “selection” operator, with a bias towards killing “bad” individuals. On

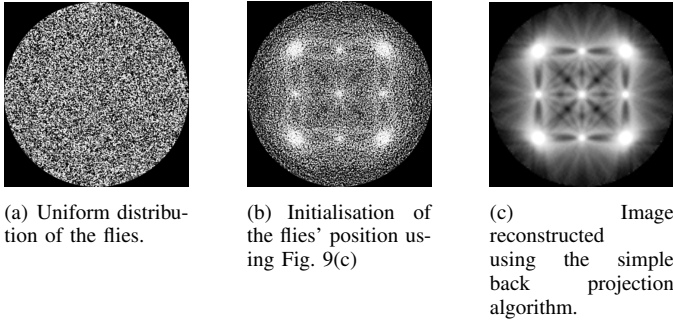


Fig. 9. Initial estimates of the reconstructed image used in Fig. 6.

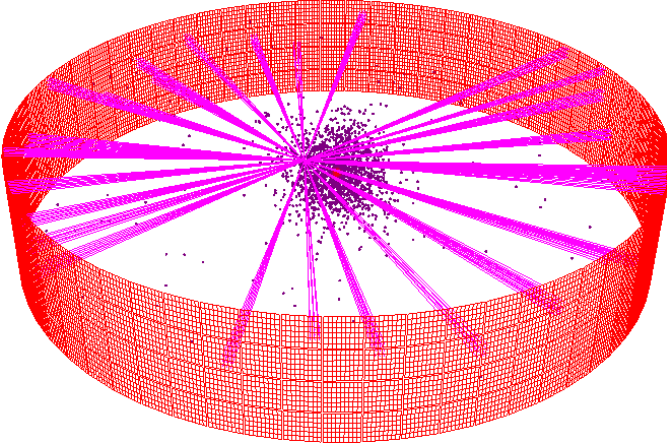


Fig. 10. Using a geometry corresponding to the GE DiscoveryTM PET-CT 690 scanner: in red crystals, last created fly's LOR in purple lines, fly's positions in coloured dots.

the other hand, if the new fly is to be created by mutation of another fly, this fly is randomly chosen by the “selection” operator, with a bias towards reproducing “good” individuals. The selection operator makes use of the local fitness, i.e. the individual fitness of flies. Classical selection operators are ranking, roulette wheel and tournament.

When we were addressing the SPECT problem, we showed that if we defined the fitness of a fly as a bonus-based function then it gave an important bias to the algorithm with a tendency of the smaller objects to disappear [14]. This is why we then introduced marginal evaluation ($F_m(i)$) to assess a given fly (i). It is based on the leave-one-out cross-validation method. We use a similar approach in PET:

$$F_m(i) = \text{dist}(\text{pop}, \text{input}) - \text{dist}(\text{pop} - \{i\}, \text{input}) \quad (1)$$

with $F_m(i)$ the marginal fitness of Fly i , $\text{dist}(A, B)$ the City block distance between two sparse matrices A and B , pop is the set of LORs simulated by the whole population, input is the set of LORs extracted from the input data, and $\text{pop} - \{i\}$ is the set of LORs simulated by the whole population without Fly i . The fitness of a given fly will only be positive when the global cost is lower (better) in presence rather than in the absence of this fly.

In our algorithm, as each fly's fitness is the value of its (negative or positive) contribution to the quality of the whole population, we managed to simplify and speed up the selection

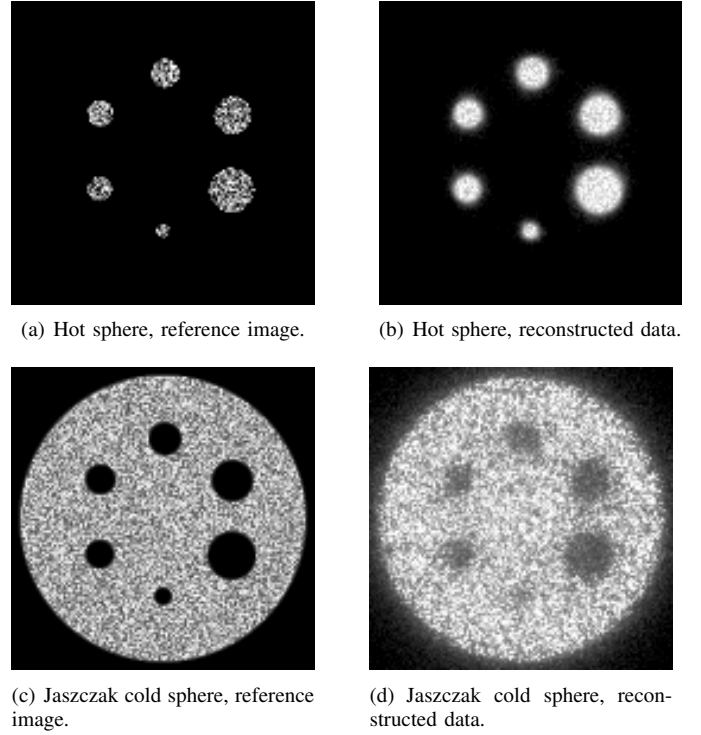


Fig. 11. 2D tomographic reconstruction of Jaszczak-inspired sphere phantoms using the Fly algorithm dedicated to PET.

process by using a fixed fitness threshold. Any “bad” fly (its fitness is negative) is a candidate for death, and any “good” fly (its fitness is positive) is a candidate for mutation. When a fly is killed, its LORs are removed from the total set of simulated LORs. When a new fly is created, its LORs are added. This process needs to be fast to be able to decrease the number of bad flies and increase the number of good flies as much as possible.

When the number of flies with a negative fitness decreases, the threshold selection fails to provide flies to be killed in an acceptable time. It also means that the reconstruction is optimum at the current resolution. If the resolution is not acceptable, then a mitosis operator is triggered to gradually increase the population size. Each fly is split into two new flies to double the population size. One of the two flies is then mutated.

E. Stopping criteria

The algorithm iterates until convergence of the estimated data with the measured data. After convergence the spatial concentration of flies will correspond to an estimate of the radionuclide concentration.

IV. RESULTS

In [15], [16], we showed the ability of the early version of the algorithm (i.e. without taking advantage of some specific genetic operators we designed in [17], [19]) to reconstruct simple 2D objects at low resolution. In [19], results at higher resolution were presented.

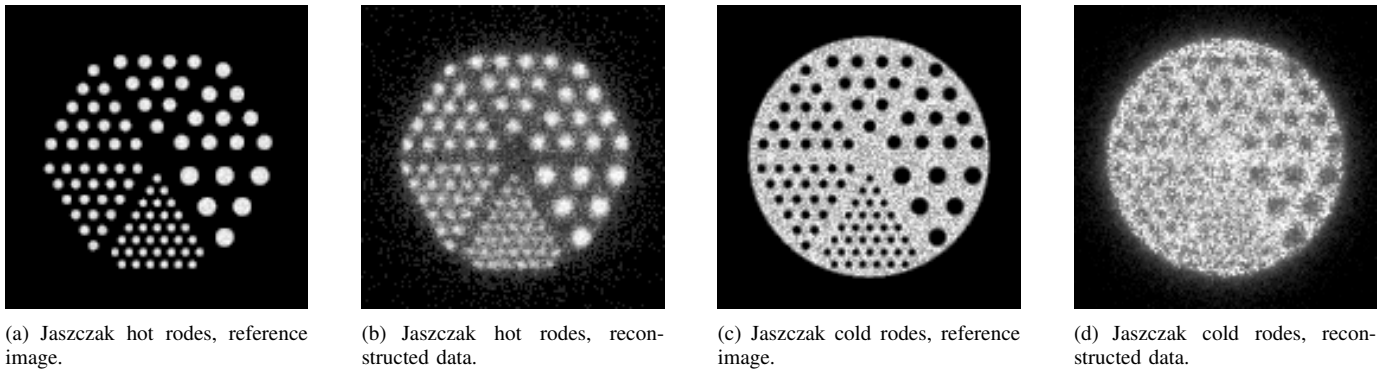


Fig. 12. 2D tomographic reconstructions of Jaszczak-inspired rode phantoms using the Fly algorithm.

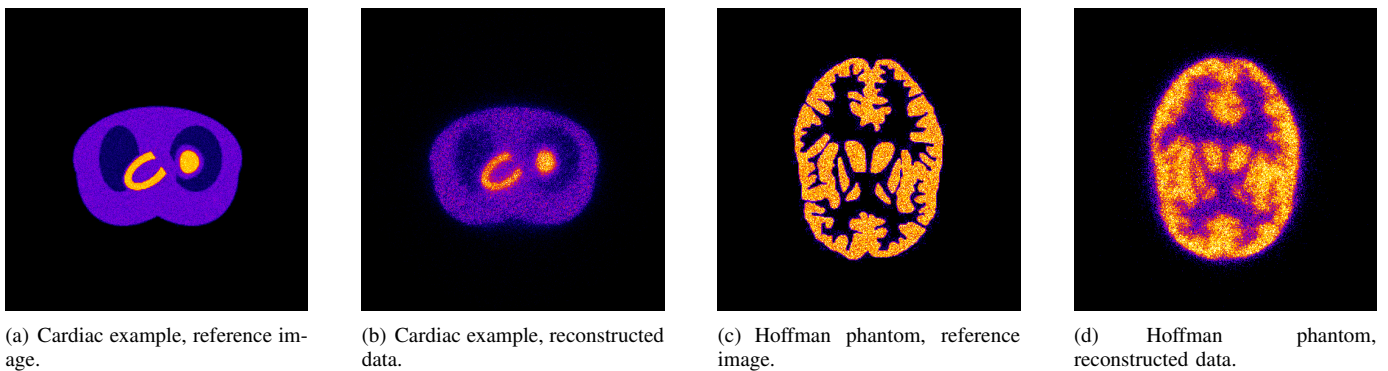


Fig. 13. 2D tomographic reconstructions of more anatomically-realistic phantoms using Fly algorithm.

This section presents new results, obtained using our specific genetic operators, with more sophisticated numerical phantoms of growing complexity. The pixel intensity is proportional to the concentration of radio-tracers.

We initially focus on the 2D case to validate qualitative results of the algorithm. No attenuation and no scattering are taken into account. A 2D scanner has been simulated. Its diameter is 85 cm, and the crystal width is 4.5 mm. The scanner is made of 72 blocks of 8 crystals each. Images in Figures 11 to 13 show raw data (i.e. no low-pass filter is applied to smooth the images) of the reference objects that have been used to generate input data, as well as the corresponding slices reconstructed using the fly algorithm. The pixel size is about $1.7 \times 1.7 \text{ mm}^2$. A series of four tests inspired of the Standard Jaszczak phantom have been used: hot and cold spheres first (see Fig. 11), then hot and cold rodes (see Fig. 12). Fig. 13 illustrates the fifth and sixth tests. They make use of more anatomically realistic models: a slice through the chest, and the Hoffman phantom (brain).

The fully-3D reconstruction of an object with a complex shape is presented in Fig. 7 and in [19]. However, only a low-resolution has been used. We now have implemented a realistic geometry based on an actual clinical PET scanner corresponding to GE DiscoveryTM PET-CT 690 (see Fig. 14). It is made of 13824 Cerium-doped Lutetium Yttrium Orthosilicate (LYSO) crystals organised in 64 sectors. Each sector contains 4 modules of a 9×6 crystals array. The crystal dimensions are $4.2 \times 25 \times 6.3 \text{ mm}^3$. The final geometry is a

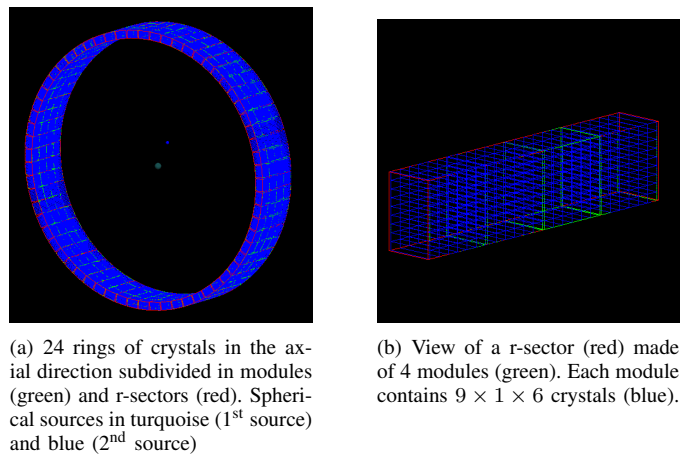


Fig. 14. Simulation of the GE DiscoveryTM PET-CT 690 using Gate.

cylinder with a ring diameter and axial field of view of 81 cm and 157 mm respectively. It is modelled using Gate, a validated medical physics simulation platform [20] dedicated to emission tomography in nuclear medicine. It is developed by the OpenGATE collaboration¹ and seats on the top of Geant4 [21]. The latter is a widely used open-source platform for nuclear physics simulation. It is developed by European Organization for Nuclear Research (CERN). The level of physics realism can be controlled. For example, in our initial test presented

¹<http://opengatecollaboration.healthgrid.org>

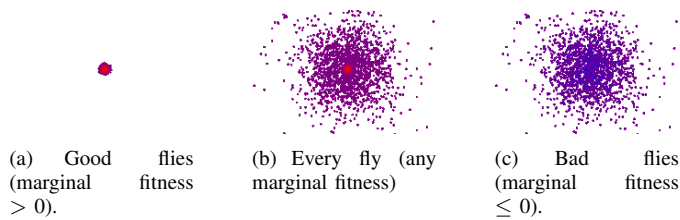


Fig. 15. Cloud of flies during the reconstruction.

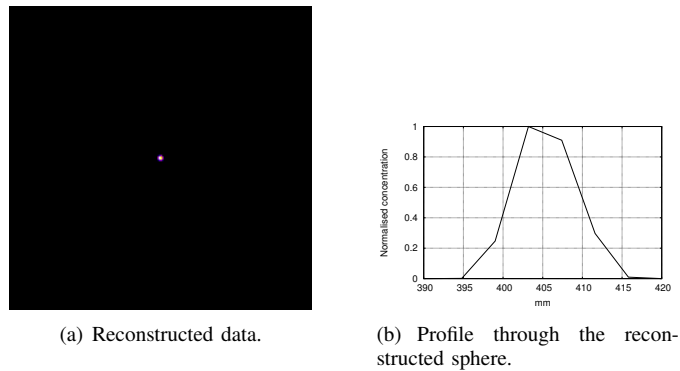


Fig. 16. PET reconstruction using the Fly algorithm.

here, Compton scattering is disabled and both “PhotoElectric” and “ElectronIonisation” are enabled to detect interactions in crystals. The aim is to generate realistic data in controlled test cases of increasing complexity. Two spherical radioactive sources of 1 megabecquerel (MBq) activity are included (see Fig. 14(a)). The first one is located at the centre of the PET system and its radius is 10 mm. The second one, whose radius is 5 mm, is shifted by 10 centimetres in each direction. It is therefore outside the field of view. Random coincidences (single photons of two different annihilations generating a LOR) are recorded and correspond to an additive noise to the data. The aim is to assess the robustness of the algorithm. About $1.3e6$ LOR in total have been recorded. Fig. 15 shows the cloud of flies at a given step in the reconstruction. As expected, only the sphere that is in the field of view of the scanner has been reconstructed. Fig. 16 shows the middle slice of the reconstructed volume and a profile corresponding to its middle line. The diameter of the reconstructed sphere is about 20 mm, which is relatively accurate.

V. CONCLUSION

This paper presented new results of positron emission tomographic reconstruction using a specific cooperative coevolution scheme based on the fly algorithm. It demonstrated the ability of the algorithm to reconstruct images using input data that corresponds to standard phantom models (the Standard Jaszczak phantom) and anatomically realistic models (cardiac and brain). However, the reconstruction of hot regions seems better than the reconstruction of cold areas; this needs to be addressed, e.g. by adding a regularisation step in the iterative process. It also showed that realistic models implemented in Gate can be used.

A comparison study with traditional reconstruction tools, such as OS-EM, will be conducted. More realistic physics

processes will be progressively added. Further work will therefore include the correction of such phenomena in the modelled system matrix, e.g. photon attenuation and Compton scattering.

ACKNOWLEDGMENTS

This work has been partially funded by FP7-PEOPLE-2012-CIG project Fly4PET – Fly Algorithm in PET Reconstruction for Radiotherapy Treatment Planning.

REFERENCES

- [1] G. L. Zeng, “Image reconstruction – a tutorial,” *Comput. Med. Imaging Graph.*, vol. 25, no. 2, pp. 97–103, 2001, DOI: 10.1016/S0895-6111(00)00059-8.
- [2] A. C. Kak and M. Slaney, *Principles of computerized tomographic imaging*. Society of Industrial and Applied Mathematics, 2001, ISBN: 978-0898714944.
- [3] S. Vandenberghe, Y. D’Asseler, R. Van de Walle, T. Kauppinen, M. Koole, L. Bouwens, K. Van Laere, I. Lemahieu, and R. A. Dierckx, “Iterative reconstruction algorithms in nuclear medicine,” *Comput. Med. Imaging Graph.*, vol. 25, pp. 105–111, 2001, DOI: 10.1016/S0895-6111(00)00060-4.
- [4] L. A. Shepp and Y. Vardi, “Maximum likelihood reconstruction for emission tomography,” *IEEE Trans. Med. Imaging*, vol. 1, no. 2, pp. 113–122, 1982, DOI: 10.1109/TMI.1982.4307558.
- [5] H. M. Hudson and R. S. Larkin, “Accelerated image reconstruction using ordered subsets of projection data,” *IEEE Trans. Med. Imaging*, vol. 13, no. 4, pp. 601–609, 1994, DOI: 10.1109/42.363108.
- [6] F. H. Fahey, “Data acquisition in PET imaging,” *J. Nucl. Med. Technol.*, vol. 30, no. 2, pp. 39–49, 2002.
- [7] R. M. Lewitt and S. Matej, “Overview of methods for image reconstruction from projections in emission computed tomography,” in *Proc. of IEEE*, vol. 91, 2003, pp. 1588–1611, DOI: 10.1109/JPROC.2003.817882.
- [8] H. Zaidi, Ed., *Quantitative Analysis in Nuclear Medicine Imaging*. Springer, 2006, ISBN: 978-0-387-23854-8.
- [9] P. A. N. Bosman and T. Alderliesten, “Evolutionary algorithms for medical simulations: a case study in minimally-invasive vascular interventions,” in *Workshops on Genetic and Evolutionary Computation 2005*, 2005, pp. 125–132, DOI: 10.1145/1102256.1102286.
- [10] S. Cagnoni, A. B. Dobrzeniecki, R. Poli, and J. C. Yanch, “Genetic algorithm-based interactive segmentation of 3D medical images,” *Image Vision Comput.*, vol. 17, no. 12, pp. 881–895, 1999, DOI: 10.1016/S0262-8856(98)00166-8.
- [11] K. Völkl, J. F. Miller, and S. L. Smith, “Multiple network CGP for the classification of mammograms,” in *EvoWorkshops 2009*, ser. LNCS, vol. 5484. Springer, 2009, pp. 405–413, DOI: 10.1007/978-3-642-01129-0_45.
- [12] T. Baeck, D. B. Fogel, and Z. Michalewicz, Eds., *Evolutionary Computation I: Basic Algorithms and Operators*. Taylor & Francis, 2000, ISBN: 978-0750306645.
- [13] J. Louchet, “Stereo analysis using individual evolution strategy,” in *Proc. ICPR’00*, 2000, p. 1908, DOI: 10.1109/ICPR.2000.905580.
- [14] A. Bousquet, J. Louchet, and J.-M. Rocchisani, “Fully three-dimensional tomographic evolutionary reconstruction in nuclear medicine,” in *Proceedings of the 8th international conference on Artificial Evolution (EA’07)*, ser. Lecture Notes in Computer Science, vol. 4926, 2007, pp. 231–242.
- [15] F. P. Vidal, D. Lazaro-Ponthus, S. Legoupil, J. Louchet, E. Lutton, and J.-M. Rocchisani, “Artificial evolution for 3D PET reconstruction,” in *Proceedings of the 9th international conference on Artificial Evolution (EA’09)*, ser. Lecture Notes in Computer Science, vol. 5975. Strasbourg, France: Springer, Heidelberg, 2010, pp. 37–48, DOI: 10.1007/978-3-642-14156-0_4.
- [16] F. P. Vidal, J. Louchet, E. Lutton, and J.-M. Rocchisani, “PET reconstruction using a cooperative coevolution strategy in LOR space,” in *IEEE Nuclear Science Symposium Conference Record*. Orlando, Florida: IEEE, Oct. 2009, pp. 3363–3366, DOI: 10.1109/NSS-MIC.2009.5401758.

- [17] F. P. Vidal, J. Louchet, J.-M. Rocchisani, and E. Lutton, "New genetic operators in the Fly algorithm: application to medical PET image reconstruction," in *European Workshop on Evolutionary Computation in Image Analysis and Signal Processing (EvoIASP'10)*, ser. Lecture Notes in Computer Science, vol. 6024, no. Part I. Istanbul, Turkey: Springer, Heidelberg, Apr. 2010, pp. 292–301, DOI: 10.1007/978-3-642-12239-2_30.
- [18] F. P. Vidal, J. Louchet, J. Rocchisani, and E. Lutton, "Flies for PET: An artificial evolution strategy for image reconstruction in nuclear medicine," *Medical Physics*, vol. 37, no. 6, p. 3139, 2010, DOI: 10.1118/1.3468200.
- [19] F. Vidal, E. Lutton, J. Louchet, and J.-M. Rocchisani, "Threshold selection, mitosis and dual mutation in cooperative co-evolution: Application to medical 3D tomography," in *Parallel Problem Solving from Nature - PPSN XI*, ser. Lecture Notes in Computer Science, R. Schaefer, C. Cotta, J. Kolodziej, and G. Rudolph, Eds., vol. 6238. Springer Berlin / Heidelberg, 2011, pp. 414–423, DOI: 10.1007/978-3-642-15844-5_42.
- [20] J. S and *et al.*, "GATE: a simulation toolkit for PET and SPECT," *Physics in Medicine and Biology*, vol. 49, pp. 4543–4561, 2004.
- [21] S. Agostinelli and *et al.*, "GEANT4 - a simulation toolkit," *Nucl. Instrum. Methods Phys. Res., Sect. A*, vol. 506, no. 3, pp. 250–303, 2003, DOI: 10.1016/S0168-9002(03)01368-8.